Research Article

Xingxing Chen, Ying Li, Ying Wang, Dingquan Song, Zuowan Zhou*, and David Hui

An approach to effectively improve the interfacial bonding of nano-perfused composites by *in situ* growth of CNTs

https://doi.org/10.1515/ntrev-2021-0025
received March 19, 2021; accepted April 24, 2021

Abstract: Nano molding technology (NMT) has shown great potential in the preparation of metal/resin composites, which can integrate resin and metal into a lightweight, high-strength metal matrix composite. However, due to the poor interfacial bonding strength between metal and polymer, the application of the metal/polymer composites is limited. In this paper, we proposed a novel method to improve the bonding strength between Fe–Co–Ni alloy and epoxy resin by Nano Perfusion Technology (NPT), featuring *in situ* growth of carbon nanotubes (CNTs) in the pores on anodized Fe–Co–Ni alloy porous surface, followed by a perfusion of epoxy resin throughout the pores that had been *in situ* grown CNTs. Due to the "anchor effect" of CNTs, the bonding strength between the epoxy and the alloy matrix is improved. The results showed that the interfacial bonding between the *in situ* CNTs-modified alloy and the resin was significantly improved compared to the metal-resin composites surface treated with T-treatment in traditional method of NMT. The maximum interfacial bonding force of the alloy-CNTs/epoxy composite reached up to 691.80 N, which was 460, 315, and 267% higher than those by mechanical treatment, without CNTs and T-treatment, respectively. This work provides a new approach to protect metals or alloys from environmental corrosion, impact damage, and so on.

Keywords: nano perfusion technology, *in situ* growth of CNTs, metal-epoxy interface bonding strength

Abbreviations

NMT	nano molding technology
CNTs	carbon nanotubes
NPT	nano perfusion technology
CVD	chemical vapor deposition
EDS	energy dispersive spectrometer
ICP-MS	inductively coupled plasma mass spectrometry

1 Introduction

Metal and resin composites have outstanding characteristics such as high strength, long fatigue life and corrosion resistance, *etc*. and are increasingly used in aerospace, automotive, and related industries. However, the bonding forces between the metal substrate and the polymeric resin metal-resin are always weak due to their opposite surficial properties [1]. Metal-resin composites are mainly produced *via* the following two technologies: metal surface crystallization and nano molding technology (NMT) [2]. Generally, through mechanical methods such as sand-blasting abrasive [3,4] or chemical etching [5,6] and anodic oxidation [7–9] on the metal surface to form micro and nano structures, the resin material is then cast into the porous surface of the metal matrix by the molding process. After the resin is cured, the metal and the polymer resin form an anchoring structure, which makes the metal-resin composite surface stronger and/or functionalized [2,10]. Later, more researchers used the anodic oxidation technique to treat metals such as magnesium [11–14] and titanium [15–18] to achieve certain micro and nano pores [19],

* **Corresponding author: Zuowan Zhou,** Key Laboratory of Advanced Technologies of Materials (Ministry of Education), School of Materials Science and Engineering, Southwest Jiaotong University, Chengdu 610031, China; Institute of Frontier Science and Technology, Southwest Jiaotong University, Chengdu 610031, China, e-mail: zwzhou@swjtu.edu.cn
Xingxing Chen, Ying Wang, Dingquan Song: Key Laboratory of Advanced Technologies of Materials (Ministry of Education), School of Materials Science and Engineering, Southwest Jiaotong University, Chengdu 610031, China
Ying Li: School of Mechanical Engineering, Chengdu University, Chengdu 610106, China
David Hui: Department of Mechanical Engineering, University of New Orleans, New Orleans, LA 70148, United States of America

which were applied in the field of energy storage or energy storage devices. However, apart from soft aluminum alloy, titanium alloy, and so on, there are few researches on other metal alloys such as iron, nickel, and chromium.

Moreover, in the process of getting metal-resin composites, in addition to nano crystallization of the metal surface, T-treatment is often used for posttreatment of anodized metal, etching the porous structure of the metal surface and interacting with the resin material so as to enhance the interfacial strength [20,21]. However, T-agents are usually amines, which are toxic and will cause harm to human body and environmental pollution in this process. Also, the mechanism by which T-agents improve the interfacial strength is still unclear.

It is well-known that the incorporation of CNTs into resin materials can improve the mechanical strength, fracture toughness, and thermal stability [22–28]. Among all kinds of reinforcing materials, carbon nanotubes have been considered as a new-generation material since the first discovery by Iijima in 1991 [29], owing to their unique properties such as ultra-high strength (up to 100 GPa), ultra-high Young's modulus (up to 1 TPa), and large aspect ratio (50–500) [30,31]. Liang *et al.* [32] proposed a novel process for preparing CNTs-reinforced magnesium nanocomposites, which combined the friction stir processing (FSP) and ultrasonic assisted extrusion. Wang *et al.* [33] showed that the mechanical properties of the Cu/CNTs composites were greatly improved after the introduction of CNTs into nanocrystalline Cu, which was attributed to the distribution characteristic of CNTs penetrating through several adjacent nano-Cu grains [34]. Although CNTs obviously enhanced the composite materials by traditional mixing and hot-consolidation process [35], the binding forces between the CNTs and metal matrix were weak, because the interfacial slip would result in reflection at a relatively low applied stress [36].

In this paper, a new strategy was proposed and realized for the first time. The CNTs were *in situ* grown on the metal surface *via* CVD after anodic oxidation, followed by a Nano-Perfusion process to obtain the alloy/CNTs/epoxy composites with high performance. First, a certain number of micro-nano pores were prepared by anodizing the surface of the alloy. Then, CNTs were synthesized by a CVD process in the anodized micro-nano pores. Finally, CNTs-modified alloy/epoxy composites were prepared by the NPT. The changes in the content of elements on the alloy surface before and after anodization were analyzed by EDS and ICP-MS, and the surface of the alloy after the growth of carbon nanotubes and the bonding of the metal-resin composite materials were characterized by a scanning electron microscope, so to have a look at the growth of carbon nanotubes and the cross-sectional morphology of the metal-resin. Carbon nanotubes were tested through XRD and Raman tests to understand the structural changes during the growth process, the bond energy between atoms on the alloy surface was tested by XPS to obtain the morphology and type of C in the grown CNT, and a universal testing machine was adopted to evaluate the bonding force of the metal-resin composite materials.

2 Experiment

2.1 Materials

The alloy used for anodic oxidation came from Chengdu Hongwei Future Electromechanical Co., Ltd. The constant voltage DC power supply (HY3500) used in the anodic oxidation process came from Shenzhen Liaofu Technology Co., Ltd. The tubular furnace FT-1200 for the growth of carbon nanotubes came from Anhui BEQ Equipment Technology Co., Ltd., using acetylene and argon gas from Chengdu Honghaoyuan Gas Co., Ltd. The epoxy resin TDE-85, accelerator (2,4,6-dimethylaminomethyl phenol), and curing agent (MethPA) used in this experiment came from Tianjin Institute of Organic Materials. In addition, graphite sheet, ammonium fluoride, ethylene glycol, sodium dihydrogen phosphate, hydrazine hydrate, acetone, and ethanol were purchased from Chengdu Chron Chemicals Co., Ltd. The reagents used in this experiment were all analytical reagents (AR) without further purification.

2.2 Two-step anodic oxidation and *in situ* growth of CNTs on alloy

The alloy to be anodized is used as the anode, and the graphite sheet is used as the cathode. In 0.1 mol/L NH_4F/ethylene glycol electrolyte, the voltage is 20 V to oxidize for 60 min to obtain one-step anodized alloy. Then the one-step anodized alloy is used as the anode, and the two-step anodized alloy is obtained by anodizing at a voltage of 20 V for 60 min in 0.1 mol/L NaH_2PO_4 electrolyte.

The alloy block after two-step anodization was put into a porcelain boat and then placed in a tube furnace. The temperature was controlled in an argon atmosphere during the whole process and was gradually raised to 650°C at a heating rate of 10°C/min, where the flow rate

of argon was 100 mL/min. Afterwards, the temperature of 650°C was kept for 30 min, during which C_2H_2 gas was introduced and the introduced C_2H_2 gas flow rate was 10 mL/min. When the temperature dropped to room temperature, the argon gas was turned off, and the alloy block was taken out for use.

2.3 Preparation of CNTs/metal/epoxy composites

10 g of TDE-85, 1 g of accelerator, and 8 g of curing agent were mixed at 40°C, and air bubbles in the stirred epoxy resin were removed by vacuum. The alloy block with *in situ* growth of CNTs was placed in a polytetrafluoroethylene mold. Then the epoxy resin material was poured into the alloy surface and cured at 170°C for 4 h and at 200°C for 1 h to obtain a NPT alloy resin composite material. Besides, the non-anodized alloy is polished with sandpaper of different meshes (80–1,200) to get a mechanically polished metal alloy block. Then the two-step anodized alloy is treated in hydrazine hydrate (T-treatment) for 30 min to obtain a T-treatment metal alloy. Then put the mechanically polished alloy and the T-treated alloy into the PTFE mold and the epoxy resin material was poured into the alloy surface of the mold. It was cured at 170°C for 4 h and at 200°C for 1 h to obtain mechanically polished and T-treated alloy resin composites. The size of the obtained metal-resin composite material is 50 mm × 10 mm × 4 mm in length, width, and thickness, and the length and width of the joint between metal and resin is 5 mm × 10 mm. The schematic diagram of composite preparation is shown in Figure 1.

2.4 Characterization

The surface morphology and EDS analysis of two-step anodized and *in situ* grown CNTs alloy were investigated *via* the scanning electron microscopy (SEM, JSM7800F) in high-vacuum mode at a voltage of 20.0 kV. Confocal Raman spectroscopy (Raman Touch), X-ray photo-electron spectroscopy (XPS, Escalab250XI), and X-ray diffraction (XRD, Bruker D8 Advance) were used to characterize the structural changes of two-step anodized alloy blocks and *in situ* grown CNTs. The XRD diffractometer used a copper target, with working voltage of 60.0 kV, current of 100.0 mA, and scanning range of 10–60°. Furthermore, the bonding properties of metal-resin composites were tested by an electronic universal testing machine (AGS-J, SHIMADZU).

3 Results and discussion

SEM observations and EDS and ICP-MS characterizations were conducted on the surface of the alloy before and

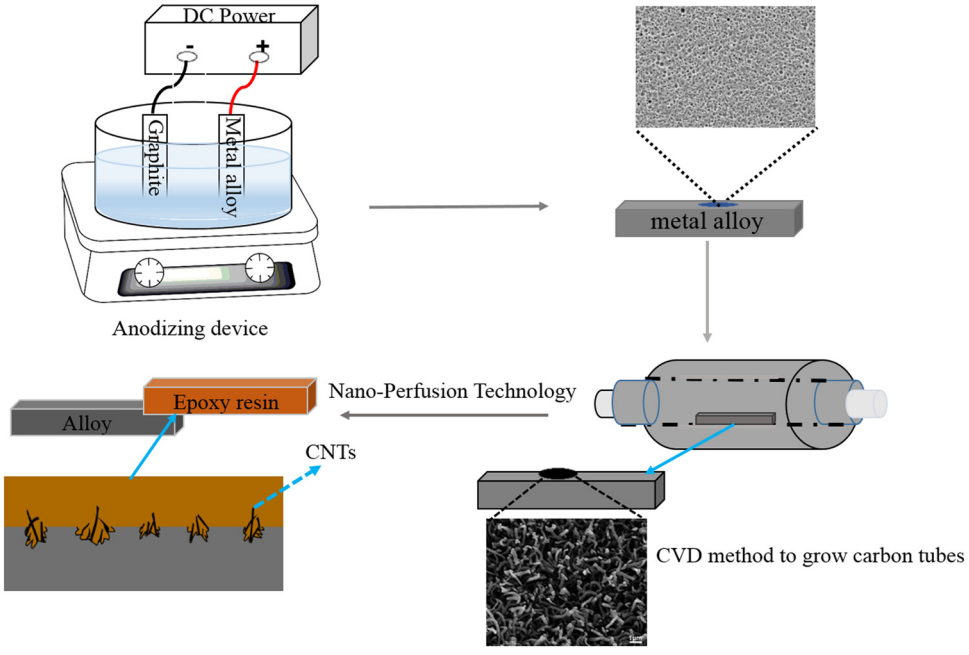

Figure 1: Schematic diagram of metal-resin composite preparation process.

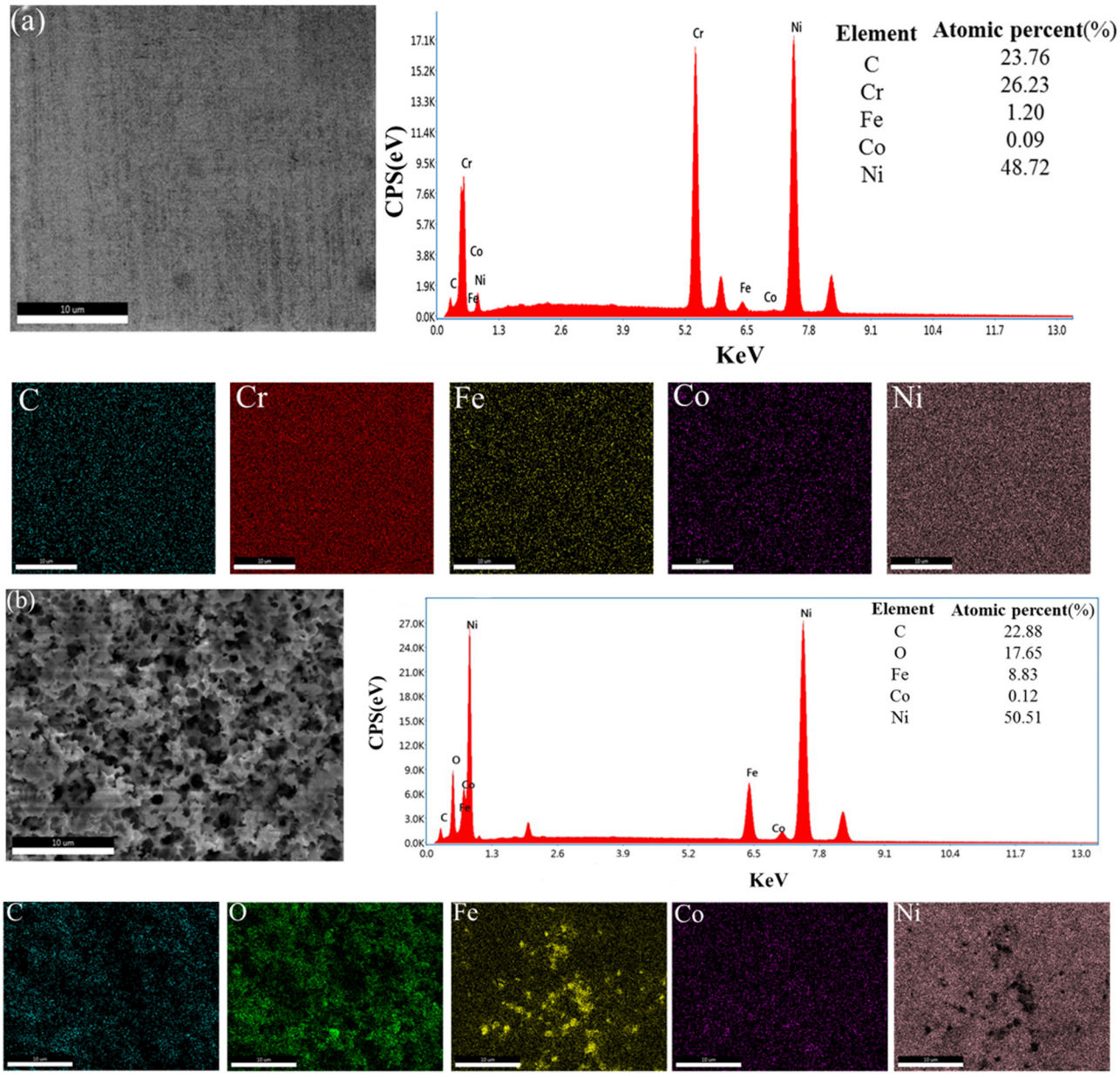

Figure 2: SEM image and EDS spectra of the alloy surface. (a) The pristine surface; (b) the surface after the two-step anodization.

after anodization, as shown in Figure 2 and Table 1. As it can be seen, the surface of the pristine alloy was smooth, but after the two-step anodization, it displayed obvious pores of micro-nano scale. The EDS analyses for the original surface shown in Figure 2(a) demonstrated that the surface contained Ni and Cr elements and a small amount

Table 1: The ICP-MS results of the pristine and after the two-step anodized samples

Sample name	Sample content (mg/kg)							
	Fe	Ni	Cr	Co	Mn	Al	Na	Cu
Pristine	826134.93	5427.59	678.53	33.91	7207.66	115.54	49.66	682.15
Two-step anodizing	800078.04	5256.27	657.12	28.16	6980.18	150.33	63.72	660.64

of Fe, Co, and C elements. After the two-step anodization, it was mainly composed of Fe–Ni. In the past, with respect to most methods for the preparation of CNTs, in order to obtain catalyst elements that can be used for the catalytic growth of CNTs, the catalyst has to be reduced first, but the alloys we used can grow CNTs *in situ* without reduction owing to the anodic oxidation treatment. The resulting porous structure exposed Fe and Ni metal components that can be used for CNTs growth, and these components can be obtained through EDS characterization, as shown in Figure 2(b). ICP-MS is used to verify the true condition of the bulk material characterization of the metal elements on the alloy surface before and after anodization. From the ICP-MS test results (Table 1), it is found that the alloy surface is still dominated by Fe and Ni after two-step anodization, which is similar to the EDS test results.

Fe [37], Co [38], Ni [39], *etc*. are usually used as catalysts for the growth of CNTs [40]. Generally, the catalyst needs to be reduced before preparation. The EDS characterization showed that after the two-step anodization, the alloy contained Fe, Ni, and other catalyst components that can catalyze the growth of CNTs, so it can catalyze the growth of CNTs without reduction. Therefore, the anodized alloy was used as a substrate for the *in situ* growth of CNTs. The alloy was placed in a tubular furnace at 650°C to change the growth time for growing CNTs *in situ*, and the surface of the alloy grown CNTs at different time was measured *via* the SEM characterization method, resulting in the SEM images of Figure 3. As shown in Figure 3(a), a certain amount of micro-nano pores can be created after the two-step anodization, while Figure 3(b) shows the morphology of the alloy block grown in the tube furnace for 10 s. It can be seen from the red framed area that CNTs grow from micro/nano pores, and the alloy surface was covered by the carbon tube arrays after 30 s of growth (Figure 3c). When the growing time reached 60 s, the diameter of the carbon tube (Figure 3d) is significantly larger than that in case of shorter growth time (Figure 3b and c). Besides, when the growth time reached 60 s, CNTs covered the entire alloy surface.

Figure 4(a) shows the XRD pattern of the CNTs grown *in situ* at different time after the two-step anodization of the alloy. As shown in Figure 4(a), there is no peak of CNTs on the anodized alloy surface at about 26° for two times, while the alloy surface of CNTs growing at different time has obvious diffraction peak at about 26°, which is similar to the (002) crystal plane of graphite, indicating that the aggregation structure of the grown products is mainly graphite structure. Besides, there are obvious Ni metal peaks around 44° and 51°, which implies that the alloy does not disappear after growth. Figure 4(b) shows the Raman spectra of the alloy after the two-anodic oxidations and after *in situ* growth of CNTs at different time. As can be seen from Figure 4, no matter the growth time is 10 s or 60 s, there are obvious D peaks and G peaks near 1,350 and 1,600 cm^{-1}, respectively, and there are obvious 2D peaks on the surface of the alloy near 2,690 cm^{-1} after

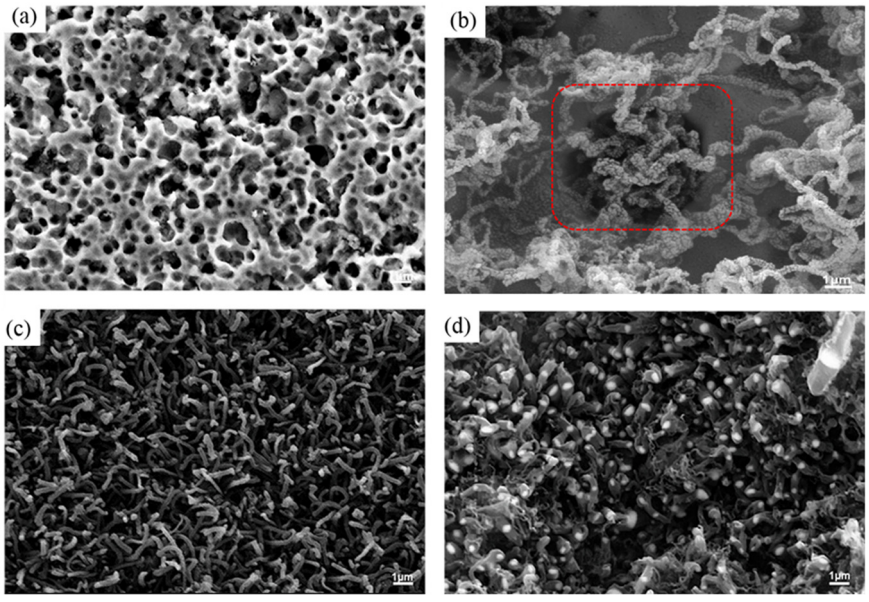

Figure 3: SEM spectra of metal substrate surface before and after the *in situ* growth of CNTs at different time. (a) Before CNTs growing; (b) growing for 10 s; (c) growing for 30 s; (d) growing for 60 s.

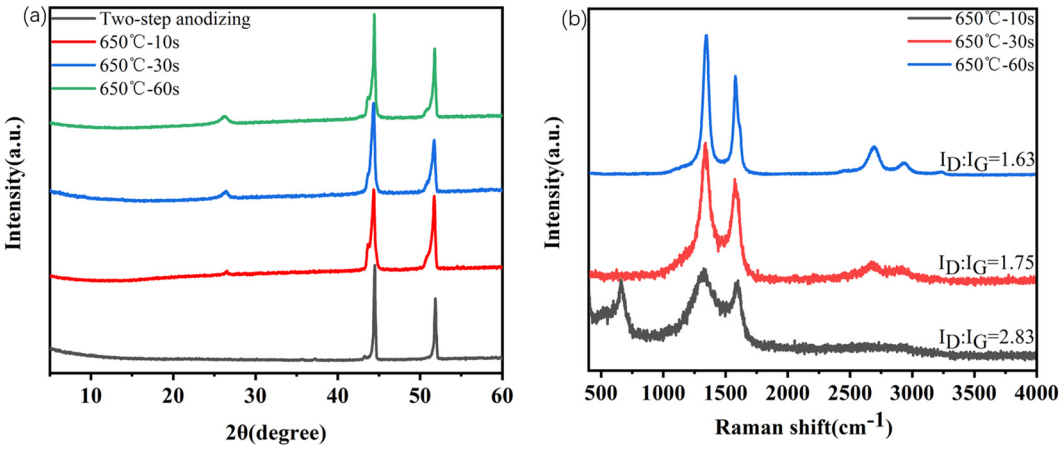

Figure 4: (a) XRD spectra of metal surface after CNTs were grown *in situ* at different time. (b) Raman spectra of metal surface after CNTs were grown *in situ* at different time.

growth of CNTs [41]. After calculating the I_D/I_G of alloy/CNTs at different growth time, it can be found that the shorter the growth time, the greater the value of I_D/I_G, which indicates that the more defects of CNTs grown *in situ* at this time, the lower the graphitization degree. As the growth time increases, the value of I_D/I_G decreased gradually, but was still greater than 1, indicating that a large number of CNTs were growing *in situ*, and a certain

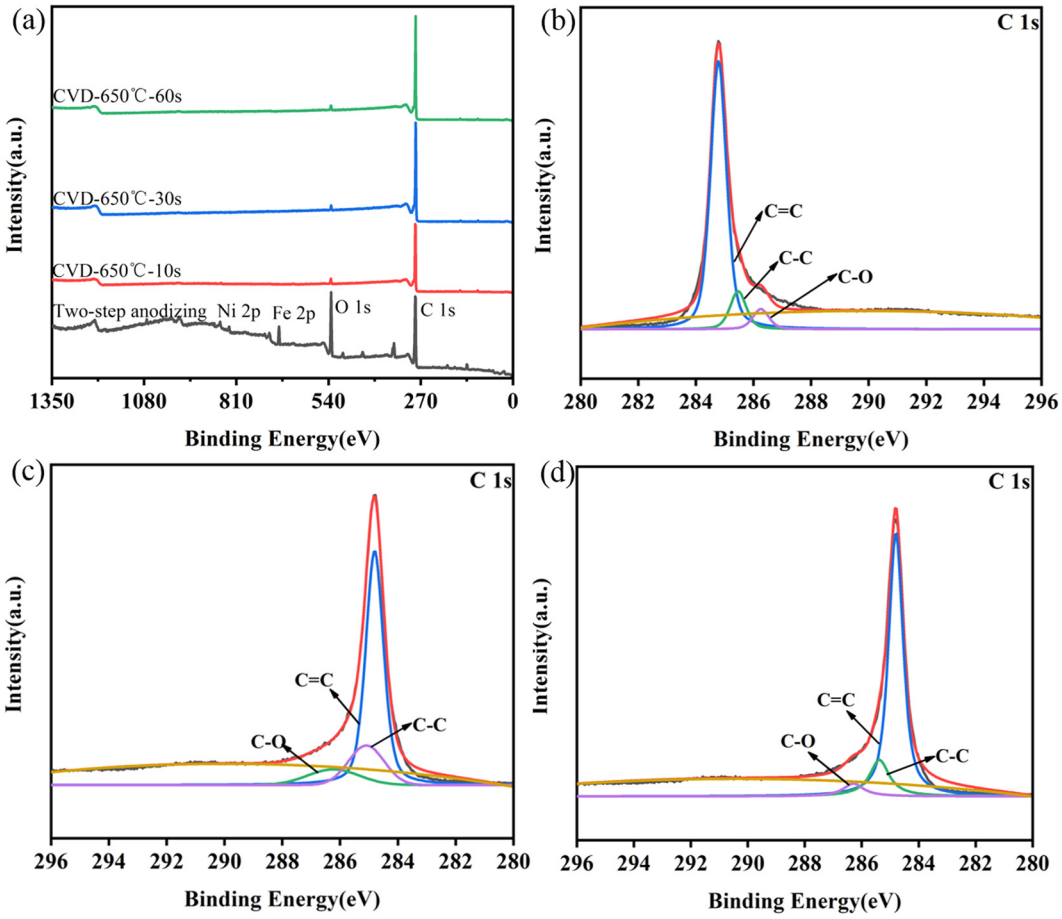

Figure 5: XPS spectra and C 1s spectra at different growth time on the surface of CNTs alloy grown *in situ* by two-step anodic oxidation. (a) Full spectrum; (b) 10 s; (c) 30 s; (d) 60 s.

force was generated by mutual extrusion between carbon tubes [42–45].

To reveal the elemental composition and electronic structure of the products after the growth of CNTs on the alloy surface, we performed XPS to characterize the composition and bonding structure of the products, and the surface of the CNTs alloy grown at different time was characterized *via* XPS, so that the XPS and C 1s spectra were obtained, as shown in Figure 5. It can be seen from the total spectrum of Figure 5(a) that the content of C atoms on the alloy surface increased from 72.71 to 98.21%, while the content of O atoms decreased from 24.31 to 1.5% after the growth of CNTs. As the growth time increases, the contents of Fe and Ni atoms on the alloy surface drop to zero, which means that the alloy surface mainly contains C and O atoms after growth. To figure out in what form the product C of carbon nanotubes grown at different time exists, the high-resolution XPS spectrum of C 1s was fitted into three subcomponents, as shown in Figure 5(b)–(d). As can be seen, when the binding energy is 284.78 eV, the C atom exists in the form of sp^2 hybridization C–C, which demonstrates that there is a graphitized structure in the carbon tube grown *in situ*. At 285.08 eV, the carbon atoms are mainly C–C formed by sp^3 hybridization, implying that there is a certain defect structure in the grown CNT. Furthermore, at 286.23 eV, it mainly exists in the form of C–O, which indicates that C and O in the grown CNT are the bonding mode of the atoms, and the resulting CNT contains oxygen functional groups [41].

After infusing epoxy resin material on the surface of the anodized alloy/CNTs with the Nano Perfusion Technology (NPT), an alloy/CNTs-epoxy composite material was obtained. At the same time, the NPT technique was adopted to inject epoxy resin material on the alloy surface after mechanical polishing, anodization, and T-treatment, so as to obtain polished alloy/epoxy composite material and anodized T-treated alloy/epoxy resin composite material. Also, the adhesion tests were carried out on the composite materials obtained by different surface treatment methods, after which the bonding performance diagram of the metal-resin composite material under different surface treatment conditions was drawn, as shown in Figure 6. It can be clearly seen from Figure 6 that the bonding force of the metal/CNTs-epoxy resin composite is the largest after the CVD method has grown for 10 s. As the growth time increases, the bonding force of the metal/CNTs-epoxy composite material decreases. But they are still greater than the interfacial bonding force of the metal-epoxy composite material obtained by methods such as unanodized, mechanical treatment, and T-treatment. In addition, it can be clearly seen from Table 2 that the bonding force of the alloy/CNTs-epoxy resin composite material is 691.80 N after CVD *in situ* growth for 10 s, the adhesive force of the metal-resin composite material after mechanical polishing is 142.32 N, and the adhesive force of the metal-resin composite material of T-treatment is 258.65 N. The other finding from Figure 6 is that no matter the growth time of 10 s, 30 s, or 60 s, the cohesive forces of metal-resin composites are much higher than those of T-treated composite materials and mechanically polished metal-resin composites.

As it can be seen from Figure 7(a), there is no obvious resin residue on the alloy surface after the bonding test of the non-anodized metal-resin composite material, while Figure 7(b)–(f) reveals obvious resin residues on the alloy surface and some CNTs still can be seen in Figure 7(d)–(f). It is shown that the interaction between the resin and the CNTs occurs after the growth of CNTs, thus allowing part of the CNT and resin to exist on the alloy surface. The main reason is that in addition to the

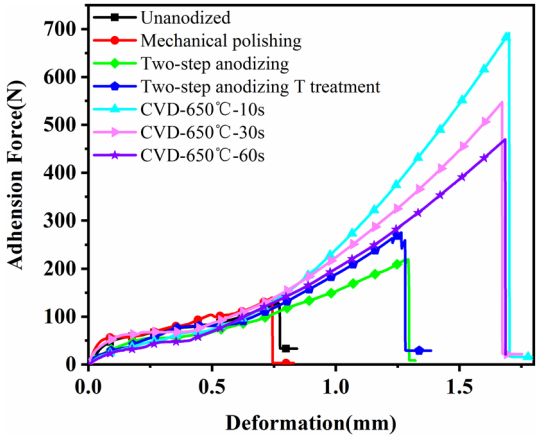

Figure 6: Test results for the adhesive force of metal-resin composites treated with different methods.

Table 2: Test results for the adhesion of metal-resin composite materials

Sample name	Adhesion force (N)
Unanodized alloy/epoxy composite	135.59
Mechanical friction alloy/epoxy composite	142.32
Two-step oxidation alloy/epoxy composite	219.22
T-treated alloy/epoxy composite	258.65
CVD-650°C-10 s	691.80
CVD-650°C-30 s	538.26
CVD-650°C-60 s	469.25

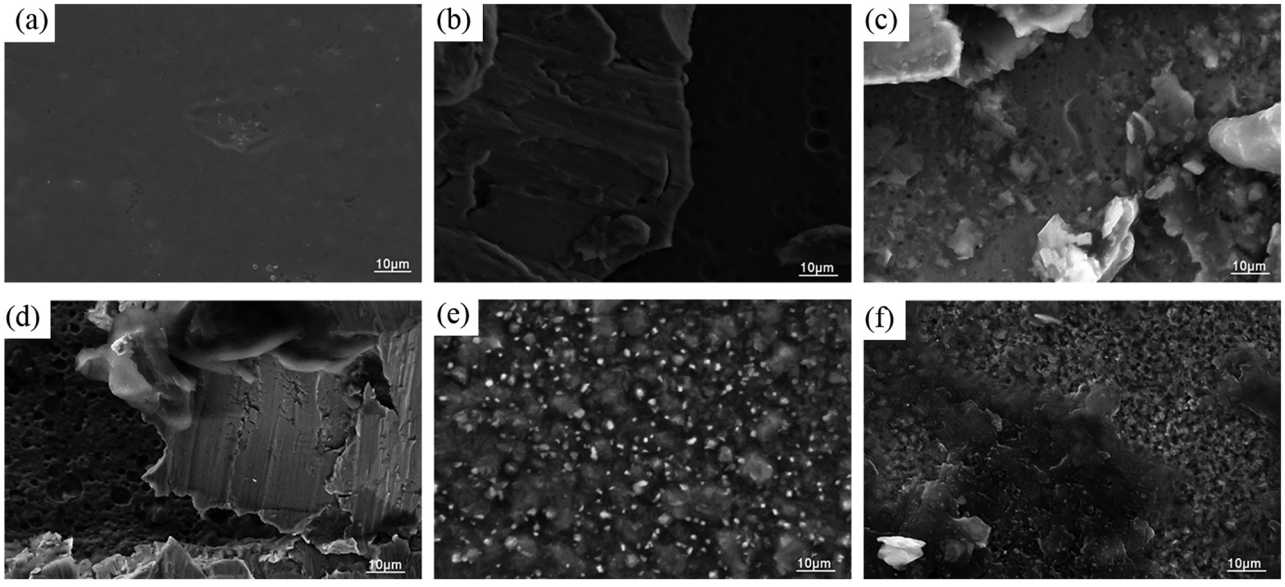

Figure 7: Surface SEM image of alloy resin composite after the bonding test. (a) Unanodized; (b) two-step anodizing; (c) T-30 min; (d) 10 s; (e) 30 s; (f) 60 s.

epoxy resin material obtained by virtue of NPT partially entering the prepared micro-nanopores, the CNTs that can be created by XPS also contain oxygen-containing functional groups, which interact with the epoxy resin, thus improving the bonding force between epoxy resin and metal/CNTs. The interaction between the CNTs grown in the pores of the alloy surface and the resin enhances the interfacial bonding force between the metal/carbon nanotubes and epoxy resin.

4 Conclusion

This paper reports a new alloy surface modification method to improve the adhesion between metal and resin materials. Different from the NMT technology, this method does not require the use of amine solutions as the so-called T-treatment, instead uses the alloy surface containing Ni, Fe, and other catalytic metal particles to directly grow carbon nanotubes *in situ*, thus modifying the surface of the alloy, and then using new NPT process to obtain the metal-resin composite materials. The results show that the *in situ* growth of CNTs on the modified alloy surface can significantly improve the adhesion between the metal and the resin, due to the "anchor effect" and the chemical interaction between CNTs and resin. When the CNTs have grown in site for 10 s, the adhesion between the metal and the resin can reach up to 691.80 N, which is much higher than 142.32 N for the alloy surface after the mechanical treatment, 219.22 N after the anodic oxidation treatment, and 258.65 N after the T-treatment. Consequently, both the *in situ* growth of CNTs and Nano Perfusion Technology (NPT) can effectively improve the adhesion between metal and epoxy resin.

Funding information: The authors gratefully acknowledge the financial support of the National Natural Science Foundation of China (No. 52002338) and the Key R&D Projects in Sichuan Province (No. 2020ZDZX0016, No. 2020ZDZX0008).

Author contributions: All authors have accepted responsibility for the entire content of this manuscript and approved its submission.

Conflict of interest: David Hui, who is the coauthor of this article, is a current Editorial Board member of *Nanotechnology Reviews*. This fact did not affect the peer-review process. The authors declare no other conflict of interest.

References

[1] Bhoi NK, Singh H, Pratap S. Developments in the aluminum metal matrix composites reinforced by micro/nano particles–a review. J Com Mater. 2020;54(6):813–33.
[2] Kadoya S, Kimura F, Kajihara Y. PBT–anodized aluminum alloy direct joining: characteristic injection speed dependence of

injected polymer replicated into nanostructures. Polym Test. 2019;75:127–32.
[3] Lucchetta G, Marinello F, Bariani PF. Aluminum sheet surface roughness correlation with adhesion in polymer metal hybrid overmolding. CIRP Ann. 2011;60(1):559–62.
[4] Kajihara Y, Tamura Y, Kimura F, Suzuki G, Nakura N, Yamaguchi E. Joining strength dependence on molding conditions and surface textures in blast-assisted metal-polymer direct joining. CIRP Ann. 2018;67(1):591–4.
[5] Fabrin PA, Hoikkanen ME, Vuorinen JE. Adhesion of thermoplastic elastomer on surface treated aluminum by injection molding. Polym Eng Sci. 2007;47(8):1187–91.
[6] Kimura F, Kadoya S, Kajihara Y. Effects of molding conditions on injection molded direct joining under various surface fine-structuring. Int J Adv Manuf Tech. 2019;101(9):2703–12.
[7] Lee W, Park S-J. Porous anodic aluminum oxide: anodization and templated synthesis of functional nanostructures. Chem Rev. 2014;114(15):7487–556.
[8] Li SM, Li YD, Zhang Y, Liu JH, Yu M. Effect of intermetallic phases on the anodic oxidation and corrosion of 5A06 aluminum alloy. Int J Min Met Mater. 2015;22(2):167–74.
[9] Zhang F, Örnek C, Nilsson J-O, Pan J. Anodisation of aluminium alloy AA7075 – Influence of intermetallic particles on anodic oxide growth. Corros Sci. 2020;164:108319.
[10] Sheikholeslami M, Farshad SA, Ebrahimpour Z, Said Z. Recent progress on flat plate solar collectors and photovoltaic systems in the presence of nanofluid: a review. J Clean Prod. 2021;1:126119.
[11] Chen Y, Lu X, Zhao F, Hu Y, Xiong S, Guo Y, et al. A study on the biocompatibility of MgO coating prepared by anodic oxidation method on magnesium metal. J Bionic Eng. 2020;17(1):76–91.
[12] Lu XY, Feng XG, Zuo Y, Zhang P, Zheng C. Improvement of protection performance of Mg-rich epoxy coating on AZ91D magnesium alloy by DC anodic oxidation. Prog Org Coat. 2017;104:188–98.
[13] Moon S, Nam Y. Anodic oxidation of Mg–Sn alloys in alkaline solutions. Cor Sci. 2012;65:494–501.
[14] Lee S, Lee D, Lee K, Park C, Lim H, Park S, et al. Evaluation of bioabsorbable Mg–Mn alloy with anodic oxidation treatment. J Nanosci Nanotechno. 2020;20(9):5625–8.
[15] Yoo SY, Park HG. Effect of anodic oxidation process parameters on TiO_2 nanotube formation in Ti-6Al-4V alloys. Korean J Met Mate. 2019;57(8):521–8.
[16] Torres-Avila IP, Padilla-Martínez II, Pérez-Hernández N, Bañuelos-Hernández AE, Velázquez JC, Castrejón-Flores JL, et al. Surface modification of the Ti-6Al-4V alloy by anodic oxidation and its effect on osteoarticular cell proliferation. Coatings. 2020;10(5):491.
[17] Hua ZK, Zhang CF, Xu YM, Jia H, Chen X, Bai Y, et al. Efficiently reduced heat rise in TiO_2 coating Ti-based metallic implants using anodic oxidation method. Surf Coat Tech. 2019;363:75–9.
[18] Chavez-Mejia AC, Zaragoza-Sanchez PI, Magana-Lopez R, Barrera-Díaz CE, Jiménez-Cisneros BE. Effect of the electrolyte chemical nature on the formation and characteristics of TiO_2 nanotubes synthesized by anodic oxidation using a Ti cathode. J Mater Sci-Mater El. 2020;31(18):15907–18.
[19] Sheikholeslami M, Farshad S. Investigation of solar collector system with turbulator considering hybrid nanoparticles. Renew Energy. 2021;171:1128–58.
[20] Rongsheng G, Guanghong H, Jian R, Yuanlong WA. Copper surface treatment in metal-polymer direct molding technology. J Shanghai Jiaotong Univ. 2021;55(1):96.
[21] Sheikholeslami M, Farshad SA, Said ZJ. Analyzing entropy and thermal behavior of nanomaterial through solar collector involving new tapes. Int Commun Heat Mass. 2021;123:105190.
[22] Mittal G, Dhand V, Rhee KY, Park SJ, Lee WR. A review on carbon nanotubes and graphene as fillers in reinforced polymer nanocomposites. J Ind Eng Chem. 2015;21:11–25.
[23] Spitalsky Z, Tasis D, Papagelis K, Galiotis C. Carbon nanotube-polymer composites: chemistry, processing, mechanical and electrical properties. Prog Polym Sci. 2010;35(3):357–401.
[24] Hong SK, Kim D, Lee S, Kim BW, Theilmann P, Park SH. Enhanced thermal and mechanical properties of carbon nanotube composites through the use of functionalized CNT-reactive polymer linkages and three-roll milling. Compos Part A-Appl Sci Manufac. 2015;77:142–6.
[25] Roy S, Petrova RS, Mitra S. Effect of carbon nanotube (CNT) functionalization in epoxy-CNT composites. Nanotechnol Rev. 2018;7(6):475–85.
[26] Visconti P, Primiceri P, de Fazio R, Ficarella A, Carlucci AP. Light-Induced ignition of Carbon Nanotubes and energetic nano-materials: a review on methods and advanced technical solutions for nanoparticles-enriched fuels combustion. Rev Adv Mater Sci. 2020;59(1):26–46.
[27] Hashim H, Salleh MS, Omar MZ. Homogenous dispersion and interfacial bonding of carbon nanotube reinforced with aluminum matrix composite: a review. Rev Adv Mater Sci. 2019;58(1):295–303.
[28] Xu H, Peng C, Yan Y, Dong F, Sun H, Yang J, et al. "All-in-one" integrated ultrathin SnS_2@ 3D multichannel carbon matrix power high-areal–capacity lithium battery anode. Carbon Energy. 2019;1(2):276–88.
[29] Iijima S. Helical microtubules of graphitic carbon. Nature. 1991;354(6348):56–8.
[30] Chen B, Li S, Imai H, Jia L, Umeda J, Takahashi M, et al. Carbon nanotube induced microstructural characteristics in powder metallurgy Al matrix composites and their effects on mechanical and conductive properties. J Alloy Compd. 2015;651:608–15.
[31] He R, Huang X, Chee M, Hao F, Dong P. Carbon-based perovskite solar cells: from single-junction to modules. Carbon Energy. 2019;1(1):109–23.
[32] Liang J, Li H, Qi L, Tian W, Li X, Chao X, et al. Fabrication and mechanical properties of CNTs/Mg composites prepared by combining friction stir processing and ultrasonic assisted extrusion. J Alloy Compd. 2017;728:282–8.
[33] Wang H, Zhang Z-H, Hu Z-Y, Song Q, Yin SP, Kang Z, et al. Improvement of interfacial interaction and mechanical properties in copper matrix composites reinforced with copper coated carbon nanotubes. Mat Sci Eng A-Struct. 2018;715:163–73.
[34] Wang H, Zhang Z-H, Hu Z-Y, Wang FC, Li SL, Korznikov E, et al. Synergistic strengthening effect of nanocrystalline copper reinforced with carbon nanotubes. Sci Rep-UK. 2016;6(1):1–8.
[35] Tsai P-C, Jeng Y-R. Technology experimental and numerical investigation into the effect of carbon nanotube buckling on the reinforcement of CNT/Cu composites. Compos Sci Technol. 2013;79:28–34.

[36] Nayan N, Shukla AK, Chandran P, Bakshi SR, Murty SV, Pant B, et al. Processing and characterization of spark plasma sintered copper/carbon nanotube composites. Mat Sci Eng A-Struct. 2017;682:229–37.
[37] Lyon JL, Stevenson KJ. Anomalous electrochemical dissolution and passivation of iron growth catalysts in carbon nanotubes. Langmuir. 2007;23(22):11311–8.
[38] Lu Q, Yu J, Zou X, Liao K, Tan P, Zhou W, et al. Self-catalyzed growth of Co, N-codoped CNTs on carbon-encased CoSx surface: a noble-metal-free bifunctional oxygen electrocatalyst for flexible solid Zn–air batteries. Adv Funct Mater. 2019;29(38):1904481.
[39] Ma Z, Wang Y, Qin J, Yao Z, Cui X, Cui B, et al. Growth of carbon nanotubes on the surface of carbon fiber using Fe–Ni bimetallic catalyst at low temperature. Ceram Int. 2021;47(2):1625–31.
[40] Pasha MA, Poursalehi R. Carbon nanotube formation over laser ablated M and M/Pd (M = Fe, Co, Ni) catalysts: the effect of Pd addition. Fuller Nanotub Car N. 2016;24(10):611–21.
[41] Jin H, Bu Y, Li J, Fen X, Dai L, Wang J, et al. Strong graphene 3D assemblies with high elastic recovery and hardness. Adv Mater. 2018;30(36):1707424.
[42] Mhamane D, Suryawanshi A, Unni SM, Rode C, Kurungot S, Ogale S, et al. Hierarchically nanoperforated graphene as a high performance electrode material for ultracapacitors. Small. 2013;9(16):2801–9.
[43] Aurbach D, Levi MD, Levi E, Teller H, Markovsky B, Salitra G, et al. Common electroanalytical behavior of Li intercalation processes into graphite and transition metal oxides. J Electrochem Soc. 1998;145(9):3024–34.
[44] Lin W, Zhang RW, Moon KS, Wong CP. Synthesis of high-quality vertically aligned carbon nanotubes on bulk copper substrate for thermal management. IEEE Trans Adv Packag. 2010;33(2):370–6.
[45] Li G, Chakrabarti S, Schulz M, Shanov V. Growth of aligned multiwalled carbon nanotubes on bulk copper substrates by chemical vapor deposition. J Mater Res. 2009;24(9):2813–20.